Global NEST Journal, **28** (4), 08721
Available online: 03/10/2026

Study on the Performance of Wheat Straw Biochar in Adsorbing Methyl Orange in Water

Funing Zhang[1, 2], Luqi Wang[1, 2], Yunqing Liu[1, 2,*], Meng Zhang[1, 2,*] and Dayi Qian[1, 2]

[1]Xinjiang Key Laboratory of Clean Conversion and High Value Utilization of Biomass Resources, Yili Normal University, Yining 835000, P.R. China
[2]Key Laboratory of Pollutant Chemistry and Environmental Treatment, School of Resources and Environment, Yili Normal University, Yining 835000, P.R. China
This work was supported by 2025 Talent Development Fund - Research and Innovation Platform Talent Team Program (XJRCSWZTD2025-6), Science and Technology Program Project of Yili Kazak Autonomous Prefecture (YJC2025B07), Tianshan Talent Training Program (2024TSYCJC0032), Yili Normal University Graduate Innovation Program Project (YSD2026CX37).

*Correspondence e-mail: liuyq151@nenu.edu.cn., zm06286022@163.com.

Abstract

Methyl orange (MO), an anionic azo dye commonly found in textile wastewater, is resistant to conventional treatment due to its refractory nature. Adsorption offers a cost-effective alternative, and wheat straw, an abundant agricultural residue, was used to prepare activated biochar. When tested with 40 mg/L MO at pH 7 and 25 °C using an adsorbent dosage of 0.10 g, the biochar achieved a maximum adsorption capacity of 17.57 mg/g and a removal efficiency of 90.04%. The adsorption followed the Langmuir isotherm ($R^2 > 0.998$), with maximum capacities ranging from 26.62 to 22.25 mg/g at 25-45 °C, and obeyed pseudo-second-order kinetics ($R^2 > 0.999$), indicating that the adsorption rate is governed by chemically driven interactions. Notably, the mesoporous structure (Type IV isotherm) and Langmuir monolayer adsorption behavior were reconciled, revealing that mesopores serve primarily as mass-transfer conduits rather than multilayer accommodation sites. This work demonstrates that KOH-activated wheat straw biochar is a cost-effective and sustainable adsorbent for anionic dye wastewater treatment, offering a viable strategy for agricultural waste valorization.

Keywords: Wheat straw biochar; Adsorption performance; Organic dye wastewater; KOH modified biochar; Isotherm and kinetic models.

OPEN ACCESS

Received: 19/06/2026,

Accepted: 14/09/2026,

Available online: 03/10/2026

Copyright: © 2026 The Author(s). Published in Global NEST Journal. This article is licensed under the terms and conditions of the Creative Commons Attribution 4.0 International license (CC BY 4.0).

Graphical abstract

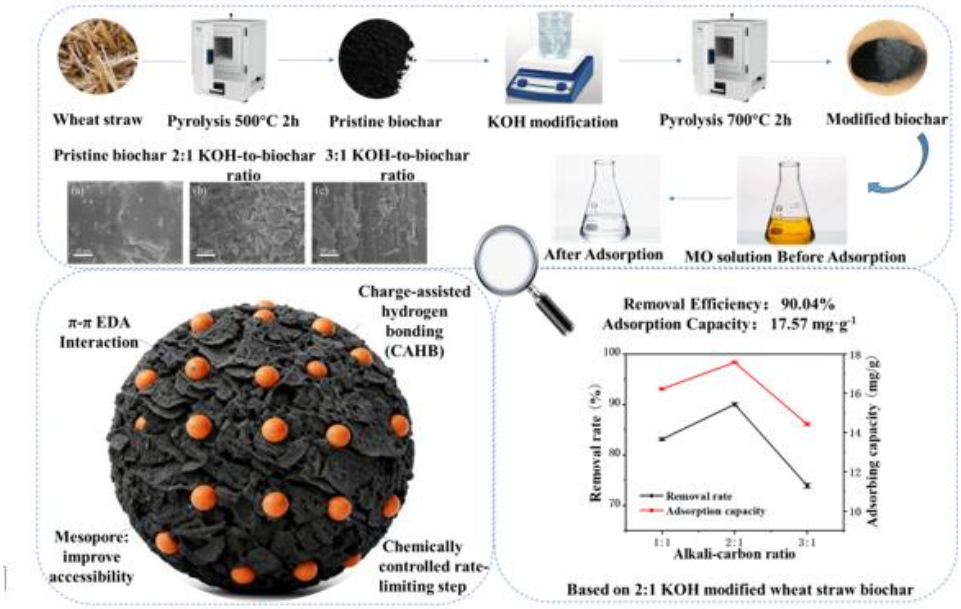

1. Introduction

Synthetic dyes are extensively used in cosmetics, printing, leather, textiles, and coatings, playing a key economic role (Moharm *et al.* 2022). Over 100,000 dyed products exist (Mim *et al.* 2023), leading to large volumes of dye wastewater. Each ton of textiles consumes 100-200 tons of water, with 80-90% discharged as wastewater containing azo dyes, sulfides, and heavy metals. Methyl orange (MO), a representative water-soluble anionic dye, belongs to the azo dye family. It is frequently utilized in textile dyeing owing to its excellent water solubility. However, its refractory nature and resistance to biodegradation make conventional wastewater treatment processes, such as coagulation, flocculation, and biological degradation often ineffective for complete removal, necessitating the development of alternative treatment technologies (Issa *et al.* 2025; Bai *et al.* 2025; Silva 2025; Lucas *et al.* 2025; Al-Rajhi *et al.* 2025; Zhao *et al.* 2023). These include adsorption-based processes using carbonaceous or clay-based materials, photocatalytic oxidation over semiconductor composites, and solar-driven Fenton oxidation in advanced reactor configurations (Nawaf *et al.* 2026a). For instance, Ag_2O/bentonite composites have been reported to achieve 99.8% organic removal from real oilfield produced water through synergistic adsorption and visible-light photocatalysis (Hassan *et al.* 2026). Among these, hybrid adsorption–photocatalytic oxidation processes have recently emerged as promising approaches for refractory organic pollutant removal (Sharshoh *et al.* 2026). The development of advanced reactor configurations, such as photocatalytic baffled reactors, has further enhanced treatment efficiency through improved mixing and light distribution (Nawaf *et al.* 2026b). Among these treatment methods, adsorption is widely used for low-concentration dye wastewater due to its cost-effectiveness, energy efficiency, and high dye recovery (Senapati *et al.* 2025). However, conventional adsorbents such as activated carbon, zeolite, and clay suffer from limited capacity and selectivity, and their high production costs further constrain large-scale application. In this context, biochar, a carbonaceous material derived from biomass pyrolysis has attracted growing interest as a low-cost and sustainable alternative (Al Saadi *et al.* 2026). Similarly, activated carbon derived from post-consumer cotton waste has been prepared via carbonization at 700 ℃, achieving a surface area of 201.3 m^2/g, and further enhanced with CuO loading for combined adsorption and photocatalytic activity (Hadi *et al.* 2026). These studies underscore the versatility of waste-derived carbon materials for wastewater treatment applications. Wheat straw is generated in large quantities globally, yet much remains underutilized and is often disposed of by open burning, causing environmental pollution and resource waste (Jamil *et al.* 2023). Chemical activation is commonly employed to enhance biochar's surface area and porosity. Among various activation agents, KOH is particularly effective in creating well-developed pore structures. For instance, KOH modification has been shown to enhance the adsorption performance of carbon-based adsorbents, increasing phenol removal from 73% to 94% on activated carbon (Humadi *et al.* 2023). Accordingly, converting wheat straw into biochar via pyrolysis followed by KOH activation offers a promising route for both agricultural residue valorization and adsorbent production (Ahmed *et al.* 2024).

Modified straw biochars have been shown to effectively remove cationic and acid dyes (Gupta *et al.* 2025; Tomin *et al.* 2024), with surface functional groups playing a key role in adsorption mechanisms (Liu *et al.* 2022). However, anionic dyes such as MO are more challenging to remove than cationic dyes because electrostatic repulsion between

the anionic dye molecules and the typically negatively charged biochar surface leads to lower adsorption affinities (Borpujari *et al.* 2025). While MO adsorption has been studied on various adsorbents, investigations using KOH-activated wheat straw biochar are still limited (Strebel *et al.* 2024). Recent studies have reported a wide range of adsorption capacities for agricultural waste-derived biochars, as summarized in **Table 1**. A brief look at recent studies reveals varied modification strategies for biochar adsorbents. Dong (Dong *et al.* 2024) achieved a 3-4 fold increase in MO adsorption via iron modification through electrostatic attraction and complexation, though equilibrium required 27 h and optimal performance was limited to acidic to neutral conditions. de Oliveira (de Oliveira *et al.*2025) demonstrated that KOH activation enabled effective removal of both cationic and anionic dyes, yet the relatively low adsorption capacity restricted its applicability to low-concentration wastewater. Abubara (Abubara *et al.*2025) showed that citric acid activation introduced abundant carboxyl and hydroxyl groups for high MB uptake, but high ionic strength significantly weakened adsorption performance via electrostatic shielding. Beyond the choice of chemical agent, the thermal conditions and impregnation ratio also critically influence pore development. Studies on desiccated coconut residue revealed that KOH activation required 600℃ with an alkali-to-biomass ratio of 1:2, whereas NaOH activation reached maximum pore development at 500℃ with a ratio of 1:3 (Yahya *et al.* 2015; Yahya *et al.* 2016). This difference arises from the distinct etching behaviors of K^+ and Na^+, the larger K^+ creates stronger pore-opening effects at higher temperatures but tends to collapse micropores when used in excess, whereas the smaller Na^+ enables more gradual pore development without structural damage even at higher impregnation ratios (Dobele *et al.* 2024). Notably, however, these studies focused exclusively on material characterization without evaluating dye adsorption performance, and thus are not included in the **Table 1**. In contrast, the present work contributes to this aspect by systematically investigating MO adsorption. Collectively, these comparisons indicate that each modification strategy presents distinct trade-offs between adsorption capacity, kinetics, pH adaptability, and salt tolerance and that the choice of activator further governs the evolution of porous structures. While single-factor optimization was employed in this study to efficiently identify the key parameters and their optimal ranges, this approach does not account for potential interactions between variables. Multivariable optimization methods such as response surface methodology (RSM) have been widely applied in recent adsorption studies to evaluate interactive effects among operating parameters and to identify true optimal conditions (Astuti *et al.* 2025; Limmun *et al.* 2025). The present work serves as a foundation for future RSM-based optimization, which could further refine the adsorption conditions and quantify parameter interactions.

Table 1. Comparison of adsorption performance of various agricultural waste-derived biochars for dye removal.

Feedstock	Modification	Dye	Performance	Key conditions	Reference
Wheat straw	KOH activation	MO	17.57 mg/g	40 mg/L, pH=7, 25 °C	This study
Rice husk	$FeCl_3$ impregnation	MO	17.2 mg/g	20 mg/L, pH=6, 25 °C	Dong *et al.* 2024
Peanut shell	$FeCl_3$ impregnation	MO	6.0 mg/g	20 mg/L, pH=6, 25 °C	Dong *et al.* 2024
Sugarcane bagasse	KOH activation	MO	95.1% removal	25 mg/L	de Oliveira *et al.* 2025
Sugarcane bagasse	KOH activation	MB	8.20 mg/g (Langmuir)	25 mg/L	de Oliveira *et al.* 2025
Prosopis juliflora waste	Citric acid activation	MB	37.6 mg/g	40 mg/L, pH=9, 25 °C	Abubara *et al.* 2025

Against this background, the present study employed wheat straw as feedstock to synthesize biochar via KOH activation and evaluated its MO removal performance. Meanwhile, the biochar exhibited stable MO removal (>90%) across pH 3-7 via π-π stacking and hydrogen bonding, with a decline above pH 7 due to OH^- competition and electrostatic repulsion, while coexisting anions (NO_3^-, SO_4^{2-}, Cl^-, HCO_3^-) caused negligible interference (variation < 3%). A suite of analytical techniques, including Fourier Transform Infrared Spectroscopy (FTIR), X-ray diffractometer (XRD), Scanning Electron Microscopy (SEM), and Brunauer–Emmett–Teller method (BET), was used to characterize the functional groups, structure, morphology, specific surface area, and pore volume of the synthesized material. The effects of KOH-to-biochar ratio, competing anions, and temperature were investigated, and the adsorption behavior was analyzed using isotherm, kinetic, and thermodynamic models. This work contributes to the field by distinguishing between the physical pore development and chemical functional group introduction associated with KOH activation, and by clarifying how these factors jointly govern anionic MO adsorption. The adsorption capacity of 17.57 mg/g, while moderate compared to activated carbon, falls within the typical range for agricultural waste-derived biochars and is achieved through π-π stacking and hydrogen bonding that overcome electrostatic repulsion, a known challenge for anionic dye adsorption. In addition, this work addresses the apparent contradiction between the mesoporous structure, as indicated by the Type IV isotherm, and Langmuir monolayer adsorption behavior, and further examines the complementary roles of surface homogeneity, reflected by the Langmuir model with R^2> 0.998, and heterogeneity, indicated by the Freundlich parameter 1/n < 1, in influencing adsorption capacity and concentration range applicability.

2. Materials and methods

2.1. *Reagents and materials*

All reagents were analytical grade and solutions were prepared with deionized water. MO, hydrochloric acid, potassium sulfate, potassium hydroxide, sodium chloride,

and sodium bicarbonate were sourced from Shanghai Maclin Biochemical Technology Co., Ltd.

2.2. *Experimental Methods*

2.2.1. Preparation of pristine biochar from wheat straw

Wheat straw was washed with distilled water and oven-dried at 80 °C for 24 h. 30g dried straw was then placed in a covered ceramic crucible and pyrolyzed in a muffle furnace at 500 °C for 2 h. After pyrolysis, the furnace was turned off and the biochar was allowed to cool naturally to room temperature to obtain pristine biochar.

2.2.2. Modification of pristine biochar

5 g of pristine biochar was mixed with KOH at mass ratios of 1:1, 2:1, and 3:1 in 125 mL deionized water, oscillated for 3 h, made the biochar fully contacted with the potassium hydroxide, and then left for 17 h after filtration, dried for 24 h. The dried mixture was placed in a muffle furnace, where it was held at 700 °C for 2 h. After the furnace cooled down to ambient temperature, the resulting product was collected and washed repeatedly with deionized water until the pH of the filtrate became neutral, as verified by pH test paper. The neutralized product was then dried for 24 h and passed through a 60-mesh sieve.

2.2.3. Characterization of pristine biochar and alkali-modified biochar

XRD, FT-IR (500-4500 cm^{-1}), SEM, and BET were used to analyze structure, functional groups, morphology, and porosity.

2.2.4. Single factor influence experiment

Effects of KOH ratio (1:1-3:1), adsorbent dosage (0.05-0.20 g), pH (3-9), anions (NO_3^-, SO_4^{2-}, Cl^-, HCO_3^-), and temperature (25-60 °C) on MO adsorption were studied.

2.3. *Adsorption property evaluation*

The adsorption rate (R) and adsorption capacity (q) were calculated according to equation (1) and (2).

$$\eta = \frac{C_0 - C_e}{C_0} \times 100\% \quad (1)$$

$$Q = \frac{(C_0 - C_e)V}{m} \quad (2)$$

η is the adsorption rate, %; Q is the adsorption capacity, mg/g; C_0 is the initial mass concentration of MO solution, mg/L; C_e is the mass concentration of MO at adsorption equilibrium, mg/L; V is the volume of MO solution, mL; *m* is the mass of the adsorbent used, g.

2.3.1. Adsorption kinetics study

MO solution (40 mg/L, 50 mL) with 0.10 g biochar was shaken at 150 r/min for 5-210 min. The filtrate was collected through 0.45 μm membrane filtration and analyzed for residual MO concentration.

(1) Pseudo-first-order and pseudo-second-order models were fitted to the kinetic data (Nascimento *et al.* 2023).

Quasi-first-order dynamics (Bandar *et al.* 2023):

$$q_t = q_e\left(1 - e^{k_1 t}\right) \quad (3)$$

Quasi-second-order dynamics (Senapati *et al.* 2025):

$$\frac{t}{q} = \frac{1}{k_2\, q_e^2} + \frac{t}{q_e} \quad (4)$$

Where: q_e- represents the equilibrium adsorption capacity (mg/g);

q_t - is the adsorption of MO by biochar at time t (mg/g);

k_1 - quasi-first-order kinetic adsorption rate constant (1/min);

k_2 - quasi-second-order kinetics g/(mg·min).

(2) The Weber-Morris intraparticle diffusion model was applied (Zhai 2023).

Weber-Morris intra-particle diffusion model(Wei *et al.* 2023):

$$q_t = k_p\sqrt{t} + C \quad (5)$$

Where: q_t - represents the adsorption amount at the time of adsorption t, mg/g;

t - adsorption time, min;

k_p - represents the diffusion constant in the particle, mg/(g·$\sqrt{\min}$);

C - represents the constant related to the thickness of the boundary layer, plotted with $\sqrt{t}$ as the horizontal coordinate and q_t as the vertical coordinate, calculated from the slope and intercept to obtain k_p and C.

2.3.2. Experimental study of isothermal adsorption

MO solutions (20-50 mg/g, 50 mL) with optimal biochar were shaken at 150 r/min and 25, 35, 45 ℃ until equilibrium. Residual MO concentration was measured, and adsorption capacity was calculated. Langmuir and Freundlich isotherm models were fitted to the equilibrium data (Majd *et al.* 2022).

Langmuir adsorption isotherm expression (Reçber 2022):

$$\frac{C_e}{q_e} = \frac{1}{K_L q_m} + \frac{C_e}{q_m} \quad (6)$$

Freundlich adsorption isotherm expression(Aider *et al.* 2023):

$$\ln q_e = \frac{1}{n}\ln C_e + \ln K_F \quad (7)$$

Where: C_e - represents the concentration of MO solution at equilibrium (mg/g);

q_m - represents the maximum equilibrium adsorption capacity (mg/g);

q_e - denotes equilibrium adsorption (mg/g);

K_L - stands for Langmuir constant;

K_F - stands for Freundlich constant.

2.3.3. Experimental study of adsorption thermodynamics

Thermodynamic parameters (ΔG, ΔH, ΔS) were calculated to assess spontaneity and heat changes (Girish *et al.*2025). The thermodynamic equations of adsorption are shown in equation (8), (9), (10)and(11).

$$k = \frac{q_e}{C_e} \tag{8}$$

$$\ln k = -\frac{\Delta H}{RT} + \frac{\Delta S}{R} \tag{9}$$

$$\Delta G = -RT\ln k \tag{10}$$

$$\Delta G = \Delta H - T\Delta S \tag{11}$$

Where: R - represents the gas constant, 8.314 J/(mol·k);

T - Kelvin Temperature, K;

ΔS - stands for entropy change.

3. Result and analysis

3.1. *Characterization result analysis*

3.1.1. FT-IR analysis

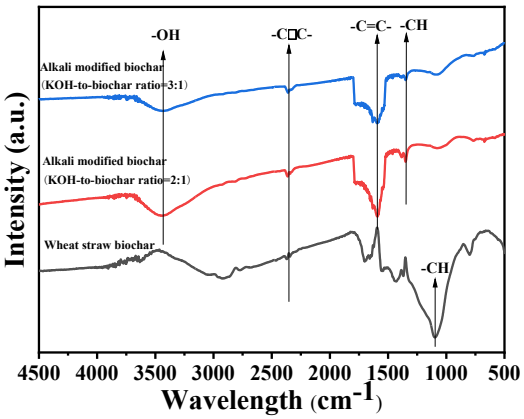

Figure 1. Infrared spectrogram of pristine biochar and two modified biochars.

FT-IR spectra of pristine and modified biochars are shown in **Figure 1**. Among the identified peaks, the one at 3444 cm^{-1} corresponds to the absorption band due to the stretching vibration of the hydroxyl (-OH) group. Meanwhile, the peak at 2356 cm^{-1} is attributed to the stretching vibration of the carbon triple bond (-C≡C-), indicating the presence of minor unsaturated carbon moieties on the biochar surface. The peaks observed at 1582 cm^{-1} are associated with the stretching vibrations of the carbon double bond (-C=C-), and those at 1348 cm^{-1} and 1083 cm^{-1} correspond to the stretching vibrations of the alkyl group (-CH) (Xu *et al.* 2022). After modification, -OH intensity decreased due to dehydration at high temperature (Dukanović *et al.* 2026). Although the -OH intensity decreased, KOH activation concurrently introduced other oxygen-containing functionalities, which still provide polar sites capable of forming charge-assisted hydrogen bonding (CAHB) with the sulfonate groups ($-SO_3^-$) of methyl orange, thereby retaining chemical affinity toward MO (Chen. *et al.* 2024; Mohammed *et al.* 2026). The broadening of the -C=C- absorption peak suggests the progression of aromatization, leading to the formation of a more condensed aromatic structure (Liu *et al.* 2023). This enhanced aromaticity indicates the development of graphitic microdomains on the biochar surface, which serve as π-electron donors for π-π electron donor-acceptor (EDA) interactions with the electron-deficient aromatic rings of methyl orange, thereby enhancing the adsorption capacity (Loebsack *et al.* 2025).

3.1.2. XRD analysis

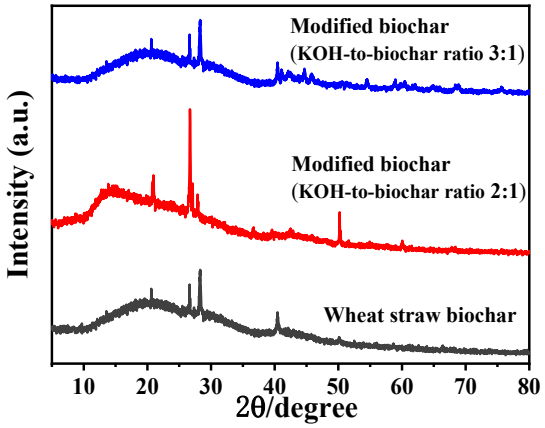

Figure 2. XRD pattern of pristine biochar and two modified biochars.

XRD patterns (**Figure 2**) showed similar features for all samples. The 3:1 sample showed weakened peaks near 2θ=40°, indicating structural damage from excessive KOH (Wang *et al.* 2023). In contrast, the 2:1 sample exhibited a broad diffuse peak at 2θ=14° , attributable to increased amorphous carbon from KOH etching (Tang *et al.* 2022). Notably, the sharp peak at 2θ = 26.67° corresponds to the (002) plane of graphitic carbon, confirming the high structural order and graphitic crystallinity of the 2:1 modified biochar (Vasilievici *et al.* 2025). This structural order provides direct crystallographic evidence for the aforementioned π-π interactions, explaining why this ratio exhibits the optimal adsorption performance (Yu *et al.* 2025). The phases corresponding to the peaks in the 2θ range of 26°-28° were identified as KCl and $K(AlSi_3O_8)$, known as potassium feldspar (Zhang *et al.* 2024; Fernandes *et al.* 2022). The potassium ions (K^+) primarily originated from the modifying agent KOH, while the chloride ions (Cl^-) likely derived from the 0.1 M dilute hydrochloric acid used in the neutralization wash. The KCl formed during the neutralization wash remained adhered to the biochar surface (Feng *et al.* 2026). The presence of KCl and potassium feldspar may exert a dual effect: K^+ can act as cation bridges to attract anionic MO, while inorganic residues may block surface active sites, reducing adsorption capacity. Moderate KCl retention on the 2:1 sample favors electrostatic attraction, whereas the higher feldspar content in the 3:1 sample, together with excessive etching, reduces the availability of active sites (Abbaci *et al.* 2022; Li *et al.* 2025).

Table 2. BET parameters of pristine biochar and two modified biochars

Materials	Specific surface area (m^2/g)	Total hole volume (cm^3/g)	Mean pore size (nm)
pristine biochar	10.14	0.067	/
Biochar with a 2:1 KOH-to-biochar ratio	87.73	0.111	10.69
Biochar with a 3:1 KOH-to-biochar ratio	34.68	0.124	4.62

3.1.3. BET analysis

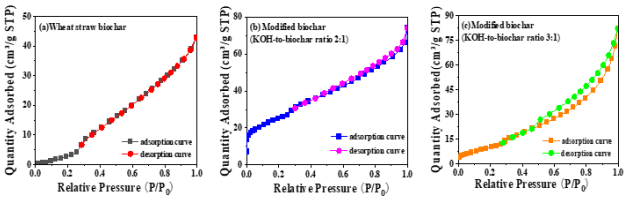

Figure 3. Adsorption and desorption curves of pristine biochar, (b) modified biochar (2:1), (c) modified biochar (3:1)

Table 2 showed specific surface area increased from 10.14 m^2 /g to 87.73 m^2 /g and 34.68 m^2 /g. This increase is attributed to KOH activation widening the pores, whereas excessive KOH merges adjacent pores into larger ones, reducing the surface area.For the 2:1 and 3:1 modified biochars, the total pore volume increased from 0.067 to 0.111 and 0.124 cm^3 /g, respectively, while the mean pore size changed from 10.69 nm (2:1) to 4.62 nm (3:1). The pristine biochar exhibited a very low specific surface area, which prevented reliable calculation of its average pore size; therefore, this value is not presented in Table 2. The pristine biochar exhibited a Type III isotherm (**Figure 3**), indicating weak interaction with MO (Hamad *et al.* 2024). Modified biochars showed Type IV isotherms with hysteresis loops, indicating mesoporous structure (Zhang *et al.* 2025). The developed mesopores provide ample accessible sites, substantially benefiting the adsorption process (Wang *et al.* 2024). Although the 3:1 sample showed a slightly higher total pore volume, its average pore size decreased sharply to 4.62 nm.This deterioration can be attributed to three combined effects of excessive KOH activation: pore collapse from over-etching of pore walls, structural damage to the carbon framework as supported by the weakened XRD peaks near 2θ = 40°, and pore blockage caused by inorganic residues including KCl and potassium feldspar occupying pore entrances (Li *et al.* 2025). The structural damage includes partial destruction of graphitic microdomains essential for π-π interactions(Liu *et al.* 2024; Nandi *et al.* 2023). The substantially increased specific surface area further enhances the accessibility of polar sites identified in FTIR analysis, allowing oxygen-containing groups to interact more effectively with MO molecules (Rasool *et al.* 2026). Given that the modified biochars exhibit substantially superior methyl orange removal performance compared to the unmodified counterpart, all subsequent adsorption kinetic studies, isotherm model fittings, and mechanistic discussions are conducted based on the biochar with a 2:1 KOH-to-biochar ratio.

3.1.4. SEM analysis

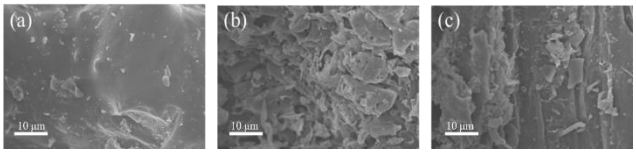

Figure 4. Scanning electron microscopy of pristine biochar before and after modification, (a) pristine biochar, (b) modified biochar (2:1), (c) modified biochar (3:1).

Figure 4 shows that the pristine biochar surface was smooth and nearly non-porous, whereas the modified biochars exhibited rough, irregular flake-like structures (Yu *et al.* 2024). The 2:1 sample exhibited more microporous and mesoporous features(Wang *et al.* 2025), in agreement with its highest specific surface area and well-developed mesoporous network from BET analysis. The 2:1 sample displayed well-defined pores with minor collapse at localized regions, likely due to the high activation temperature (700℃), whereas the 3:1 sample showed more severe structural deterioration, consistent with XRD evidence of excessive etching and graphitic domain destruction (Chang *et al.* 2025).

3.2. *Effects of different factors on the adsorption of MO by wheat straw biochar*

3.2.1. Effect of KOH-to-biochar ratio on adsorption efficiency

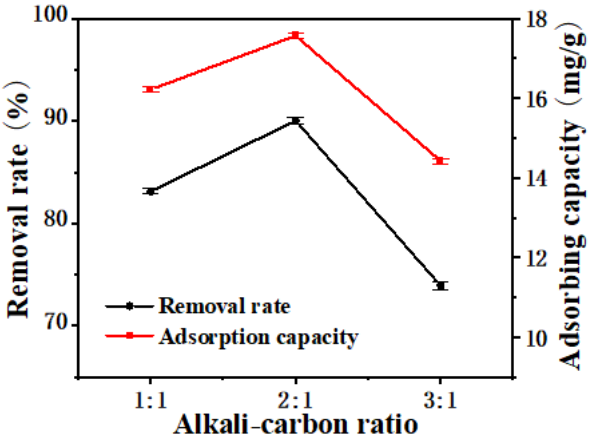

Figure 5. Effect of KOH-to-biochar ratio on adsorption effect (Data points represent mean values (n = 3), and error bars indicate standard deviations).

Figure 5 shows the effect of KOH-to-biochar ratio on MO adsorption. The removal rate increased from 83.13% at a 1:1 ratio to a peak of 90.04% at a 2:1 ratio, then declined to 73.91% at a 3:1 ratio. Similarly, the adsorption capacity rose from 16.22 mg/g to a maximum of 17.57 mg/g, before decreasing to 14.42 mg/g. Optimal performance at 2:1

ratio is due to sufficient pore expansion. However, beyond this ratio, the concentrated KOH solution begins to degrade and corrode the pore structure, leading to pore collapse and a consequent decrease in adsorption capacity(Yu *et al.* 2024).

3.2.2. Effect of dosage on adsorption effect

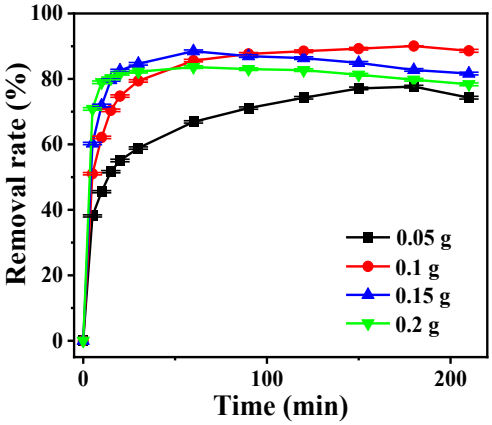

Figure 6. Effect of dosage on adsorption effect (Data points represent mean values (n = 3), and error bars indicate standard deviations).

Figure 6 shows the trend of adsorption over time for varying dosages of biochar. Notably, dosages of 0.05 and 0.10 g achieved peak removal rates and adsorption capacities at 180 min, while higher dosages of 0.15 and 0.20 g reached their maximum adsorption capacity at the 60 min mark. Increasing dosage from 0.05 to 0.10 g enhanced adsorption due to more available binding sites (Abdu *et al.* 2024). Further increase to 0.15 g reduced adsorption due to site saturation. Thus, 0.10 g was the optimal dosage.

3.2.3. The effect of pH on the adsorption effect

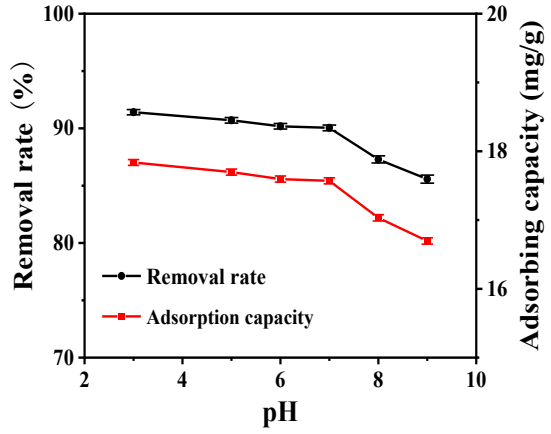

Figure 7. Effect of pH value on adsorption effect(Data points represent mean values (n = 3), and error bars indicate standard deviations).

The effect of pH on MO adsorption onto the modified biochar (2:1) is shown in **Figure 7**. In the pH range of 3-7, the adsorption remained relatively stable, with removal efficiency consistently exceeding 90%. Despite the anionic nature of MO species at pH > 3.7 (pKa ≈ 3.7), the adsorption remained stable in the pH range of 3.0 – 7.0. This stability is attributed to non-electrostatic Chemically driven interactions primarily π-π stacking and hydrogen bonding， which are sufficiently strong to overcome any potential electrostatic repulsion (Guo *et al.* 2023; Chen *et al.* 2024). However, further increasing pH beyond 7 led to a sharp decline in both removal efficiency and adsorption capacity. This decline is attributed to competitive occupation of active sites by OH^- ions (Martínez *et al.* 2023), combined with enhanced electrostatic repulsion as the progressively deprotonated biochar surface encounters increasing concentrations of anionic MO species at higher pH (Alasmary *et al.* 2025).

3.2.4. Effect of different anions on the adsorption effect

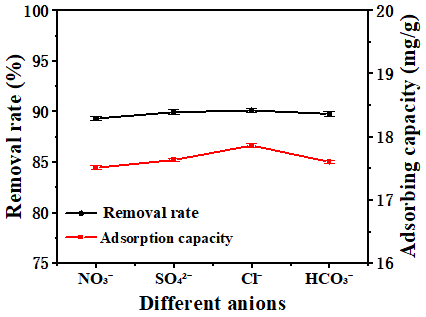

Figure 8. Effect of different anions on adsorption(Data points represent mean values (n = 3), and error bars indicate standard deviations).

To clarify the effects of these anions on adsorption performance, the current research specifically investigated how $NaNO_3$, Na_2SO_4, NaCl, and $NaHCO_3$ affect the adsorption of MO by wheat straw biochar. **Figure 8** shows that removal efficiencies in the presence of different anions were all approximately 90%, with a maximum variation of less than 3% among them. This small fluctuation falls within the experimental error range (＜ 3%), indicating that the presence of these anions has no significant impact on MO adsorption under the tested conditions.

3.2.5. Effect of temperature on the adsorption effect

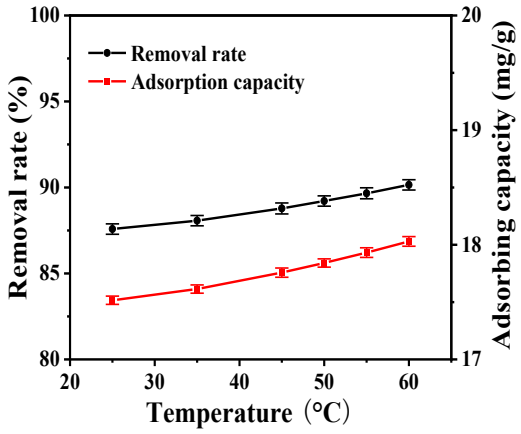

Figure 9. Effect of temperature on adsorption effect (Data points represent mean values (n = 3), and error bars indicate standard deviations).

Table 3. Quasi-first-order and quasi-second-order kinetic fitting data of biochar adsorption

Dynamic adsorption model	q_t (mg/g)	q_e (mg/g)	k_1 (1/min)	k_2 (g/mg·min)	R^2
Pseudo-first-order kinetics	17.57	16.87	0.13	/	0.974
Pseudo-second-order kinetics	17.57	17.92	/	1.28	0.999

Table 4. Fitting parameters of Weber-Morris intraparticle diffusion model.

k_{1p}	C	R^2	k_{2p}	C	R^2	k_{3p}	C	R^2
1.731	6.524	0.957	0.155	15.554	0.981	-0.265	21.127	0.999

Table 5. Langmuir and Freundlich adsorption isotherm fitting data at different temperature.

T/K	Langmuir model			Freundlich model		
	q_m/(mg/g)	K_L/(L/mg)	R^2	1/n	K_F/(mg/[g·(L/mg)^(1/n)])	R^2
298	26.62	0.52	0.998	0.22	2.53	0.979
308	23.92	1.74	0.999	0.15	2.71	0.956
318	22.25	2.90	0.999	0.11	2.77	0.967

Figure 9 shows that removal efficiency and adsorption capacity increased with temperature. At this optimum temperature, the maximum removal efficiency reached 90.15% with a corresponding adsorption capacity of 18.029 mg/g. This is due to increased Brownian motion and molecular kinetic energy. The increased kinetic energy leads to a higher frequency of collisions between the dye molecules and the biochar surface, which accelerates the adsorption process(Onyango *et al.* 2025). Elevated temperature also enhances active site reactivity. This facilitates chemical interactions, improving adsorption.

3.3. *Mechanism of MO adsorption by wheat straw biochar*

3.3.1. Adsorption kinetic analysis

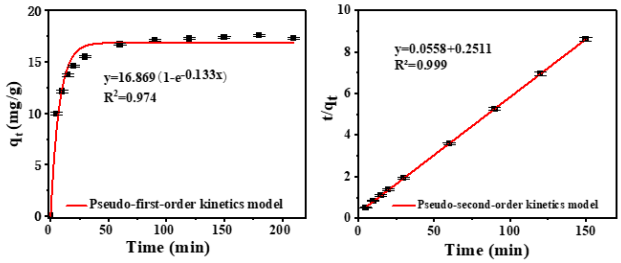

Figure 10. Adsorption kinetics, (a) pseudo-first-order kinetics; (b) pseudo -second-order kinetics. (Data points represent mean values (n = 3), and error bars indicate standard deviations)

Adsorption kinetics were fitted using pseudo-first-order and pseudo-second-order models, as shown in **Figure 10,** Table 3. The pseudo-second-order model (R^2=0.999) showed better fit than the pseudo-first-order model (R^2=0.974). This enhanced correlation indicates that the pseudo-second-order kinetic model more accurately captures the adsorption process, where the rate-limiting step is governed by chemically driven interactions (Minaei *et al.* 2024). Combined with the pH-dependent results and literature reports (Guo *et al.* 2023), this chemically rate-controlling behavior can be attributed to multiple strong non-covalent interactions between the adsorbent and adsorbate, primarily including π-π stacking between the aromatic rings of methyl orange and the graphitic microdomains of biochar, as well as charge-assisted hydrogen bonding (CAHB) between surface oxygen-containing groups and the sulfonate groups of the dye (Chen *et al.* 2024), while physical diffusion also contributes to the initial approach of dye molecules toward the active sites (Bbumba *et al.* 2025).

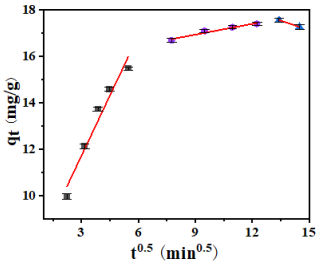

Figure 11. Weber-Morris intraparticle diffusion model(Data points represent mean values (n = 3), and error bars indicate standard deviations).

The Weber-Morris intraparticle diffusion model was applied (**Figure 11, Table 4**). The model fitting revealed a three-stage linear diffusion process, MO molecules were first quickly captured on the external surface and macropores with an extremely high diffusion rate, followed by a slower phase controlled by intraparticle transport through mesoporous and microporous structures, and finally an equilibrium phase characterized by adsorption site saturation and dynamic adsorption-desorption balance(Song *et al.* 2025; Wang *et al.* 2022). The line does not pass through the origin, indicating intraparticle diffusion is not the sole rate-limiting step (Saranya *et al.* 2022). This also indicates that external mass transfer contributes to the rate-limiting step.

3.3.2. Isothermal adsorption analysis

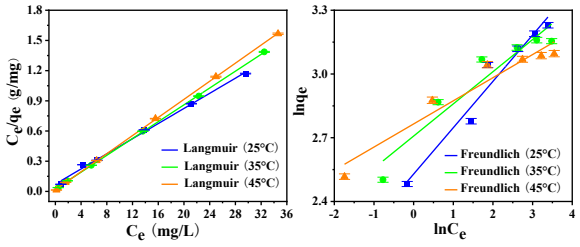

Figure 12. Isothermal adsorption model at different temperatures, (a) Langmuir model; (b) Freundlich model(Data points represent mean values (n = 3), and error bars indicate standard deviations).

Langmuir and Freundlich isotherm models were fitted to the equilibrium data. The fitting results are shown in **Figure 12 and Table 5**, The Langmuir model demonstrated superior fitting performance with remarkably high correlation coefficients (R^2 > 0.998) across all temperatures. This strongly indicates that monolayer adsorption dominates the process on relatively homogeneous surfaces (Rangasamy *et al.* 2026). Notably, this monolayer behavior does not contradict the mesoporous nature revealed by N_2 adsorption. Rather, the Langmuir model's exceptional fitting performance (R^2 > 0.998) implies, by its underlying assumption of 1:1 site-to-adsorbate stoichiometry, that the adsorption capacity is inherently limited by the number of surface active sites, rather than the physical pore volume (Lotfy *et al.* 2026). However, the Freundlich parameter 1/n < 1 under all tested conditions complements the Langmuir monolayer mechanism by implying minor secondary sites or structural defects of slightly lower energy, whose heterogeneity may favorably broaden the applicable concentration range. (Vásquez Llanos *et al.* 2025) It is worth noting that the maximum Langmuir adsorption capacity (q_m) decreased slightly with increasing temperature, from 26.62 mg/g at 25 °C to 22.25 mg/g at 45 °C. This apparent contradiction with the improved removal efficiency observed at higher temperatures can be reconciled by distinguishing equilibrium capacity from kinetic performance (Trazzi *et al.* 2024). The Langmuir q_m reflects the intrinsic affinity at equilibrium, while the enhanced uptake observed in batch experiments at elevated temperatures is mainly attributed to faster diffusion, lower viscosity, and more frequent collisions, all of which are kinetic factors that accelerate adsorption without altering the equilibrium capacity (Aziz *et al.* 2024). The slight decline in q_m suggests a mildly exothermic nature, yet the kinetic benefits of rising temperature outweigh this thermodynamic limitation under the tested conditions (Nguyen *et al.* 2025).

3.3.3. Thermodynamic analysis of adsorption

Thermodynamic parameters for MO adsorption onto the modified biochar are presented in Table 6. The negative Gibbs free energy (ΔG) at all tested temperatures confirms the spontaneous nature of the adsorption process. The positive enthalpy change (ΔH) is consistent with chemically driven interactions, supporting the endothermic and spontaneous nature of the adsorption process. (Abegunde *et al.* 2024; Ud Din *et al.* 2025). The positive entropy change (ΔS) indicates increased randomness at the solid–liquid interface (Soudagar *et al.* 2022). The ΔG becomes more negative with increasing temperature, confirming that higher temperatures favor adsorption (Benhadj *et al.* 2023). This trend is consistent with the relationship ΔG = ΔH – TΔS, where the positive ΔH and ΔS collectively drive the entropy-favored process at elevated temperatures. While the thermodynamic analysis confirmed the spontaneous and endothermic nature of the adsorption process, the practical applicability of the biochar must be further evaluated under realistic conditions, as discussed below.

Table 6. Adsorption thermodynamic fitting data.

Dye	T(℃)	R(J/mol/k)	△H (kJ/mol)	△S (J/(mol·K))	△G (kJ/mol)
MO	25	8.314	69.771	245.491	-3.288
	35				-6.244
	45				-8.442

3.4. *Challenges for real wastewater application*

While this study demonstrates effective MO removal from synthetic aqueous solutions, several challenges must be considered for practical wastewater treatment. Real textile effluents contain not only target dyes but also competing organic matter, inorganic salts, and variable pH conditions that may significantly influence adsorption performance through competitive occupation of active sites, pore blockage, and altered electrostatic interactions.

Recent studies have evaluated biochar performance using actual textile wastewater. Shah and Patel (Shah *et al.* 2026) prepared phosphorus-modified cotton stalk biochar (PCS800) for real textile wastewater treatment, achieving 60% COD removal and over 90% decolorization under optimized conditions (33 min, 6.43 g/L dosage), though this was lower than the 77% removal observed in synthetic wastewater. This performance gap highlights the challenges posed by real wastewater matrices. Adeola and Gora (Adeola *et al.* 2026) further noted that over 90% of adsorption studies remain at the laboratory scale, with fewer than 5% reaching full-scale implementation, underscoring the gap between laboratory findings and practical application.

These challenges highlight the need for further evaluation of the biochar under realistic conditions, particularly regarding the transition from laboratory-scale batch experiments to practical continuous-flow applications.

4. Conclusions

In conclusion, the KOH-activated wheat straw biochar prepared at a 2:1 ratio was systematically evaluated for MO removal. Characterization by BET, FTIR, XRD, and SEM confirmed that KOH activation substantially enhanced the specific surface area (from 10.14 to 87.73 m^2/g), introduced oxygen-containing functional groups, and developed a well-defined mesoporous structure. Under optimized batch conditions with 40 mg/L MO at pH 7 and 25 °C using 0.10 g adsorbent, the biochar achieved an adsorption capacity of 17.57 mg/g and a removal efficiency of 90.04%. The Langmuir isotherm provided the best fit (R^2 > 0.998), with capacities decreasing from 26.62 to 22.25 mg/g as temperature rose from 25 to 45 °C. The pseudo-second-order kinetics (R^2 > 0.999) and thermodynamic parameter (ΔH = 69.771 kJ/mol) jointly confirmed chemisorption as the rate-controlling step. The overall adsorption mechanism is characterized by the synergistic

effect of chemically driven interactions (π-π stacking and hydrogen bonding) and mesopore-facilitated mass transfer, where the mesopores enhance dye accessibility to active sites rather than contributing to capacity through multilayer formation. This study demonstrates that the prepared biochar offers a cost-effective and sustainable option for anionic dye wastewater treatment while enabling agricultural residue reuse. However, the experiments were conducted using single-factor optimization runs without considering multi-factor interactions, and only under controlled laboratory conditions using synthetic MO solutions, without addressing the complexity of real textile wastewater, as further discussed in Section 3.4. Future work should therefore incorporate multivariable optimization approaches to further refine the adsorption conditions, and focus on practical application aspects, including evaluation of adsorption performance using real textile wastewater, development of continuous-flow column systems for scale-up, exploration of composite modification strategies to enhance capacity, and assessment of regeneration potential and cost-effectiveness.

Author contribution

Yunqing Liu contributed to the conceptualization and methodology of the study. Guimei Yang was responsible for the data collection and analysis. Funing Zhang and Luqi Wang played a significant role in the investigation and resources. Meng Zhang, as the corresponding author, supervised the project and provided critical revisions to the manuscript. Dayi Qian contributed to the writing and editing of the paper.

Funding

We gratefully acknowledge the generous support provided by the “2025 Talent Development Fund - Research and Innovation Platform Talent Team Program (XJRCSWZTD2025-6), Science and Technology Program Project of Yili Kazak Autonomous Prefecture (YJC2025B07), Tianshan Talent Training Program (2024TSYCJC0032), Yili Normal University Graduate Innovation Program Project (YSD2026CX37)”.

Data availability

The data used and analyzed during the current study are available from the corresponding author upon reasonable request.

Consent for publication

All the authors agreed to publish the data in this journal.

Competing interests

The authors declare no competing interests.

References

Abbaci F., Nait-Merzoug A., Guellati O., Harat A., El Haskouri J., Delhalle J., Mekhalif Z., Guerrioune M. (2022), Bio/KOH ratio effect on activated biochar and their dye based wastewater depollution. J. Anal. Appl. Pyrolysis. 162, 105452.

Abdu M., Babae S., Worku A., Msagati T.A.M., Nure J.F. (2024), The development of Giant reed biochar for adsorption of Basic Blue 41 and Eriochrome Black T. azo dyes from wastewater. Sci. Rep., 14(1), 18320.

Abegunde S.M., Idowu K.S., Adubiaro H.O. (2024), Methyl Green Dye Adsorption from Wastewater Using Coconut Husk Biosorbents: Kinetic, Isotherm and Thermodynamic Studies, Iran. J. Sci., 48(1), 113-126.

Abuabara A., Diaz-Uribe C., Vallejo W., Duran F., Mosquera-Vargas E. (2025), Kinetic and thermodynamic study of cationic dye removal using activated biochar synthesized from Prosopis juliflora waste. ChemEngineering, 9(3), 64.

Adeola A.O., Gora S. (2026), Advances in physicochemical and biological treatment of textile wastewater: An applied review of methods, technologies, and costs. Water Environ. Res., 98, e70490.

Ahmed S.F., Mehejabin F., Chowdhury A.A., Almomani F., Khan N.A., Badruddin I.A., Kamangar S. (2024), Biochar produced from waste-based feedstocks: Mechanisms, affecting factors, economy, utilization, challenges, and prospects. Glob. Change Biol. Bioenergy, 16, 13175.

Aider N., Djebarri B., Touahra F., Halliche D. (2023), Adsorptive removal of methyl orange from aqueous solution by hydrotalcite derived catalysts, Desalin. Water Treat., 316, 185-197.

Alasmary Z., Akanji M.A. (2025), Iron-modified biochar derived from poultry manure for efficient removal of methyl orange dye from aqueous solution. Sustainability, 17, 6008.

Al-Rajhi A.M.H., Abdelghany T.M. (2025), Innovative strategies for wastewater treatment: harnessing green technologies for sustainable resource recovery. A review. Front. Environ. Sci., 13, Article 1696485.

Al Saadi A., Al-Yahmadi I., Al-Rashdi N., Mohamed I. I., Al-Busaidi I. K. (2026), Valorising mesquite biochar as a sustainable adsorbent for wastewater treatment: A critical review. Front. Chem. Eng., 7, 1748096.

Astuti D.N., Natsir T.A., Kristiani A., Suratman A. (2025), Electrospun PAN/Biochar okara nanofibers for efficient oxytetracycline removal: Process optimization via response surface methodology and antibacterial evaluation. Environ. Res., 284, 122238.

Aziz S., Anbreen S., Iftikhar I., Fatima T., Iftikhar A., Ali L. (2024), Green technology: synthesis of iron-modified biochar derived from pine cones to remove azithromycin and ciprofloxacin from water. Front. Environ. Sci., 12, 1353267.

Bandar K.B., Aljlil S. (2023), Utilization of Prepared Nanocellulose as a Biopolymer for Adsorption Kinetics of Cobalt Ions from Wastewater, Polymers, 15(9), 2143.

Bai X., Li C., He S., Zhou J., Jia H. (2025), Combining advanced oxidation processes with biological processes in organic wastewater treatment: Recent developments, trends, and advances. Desalin. Water Treat., 323, Article 101263.

Bbumba S., Karume I., Kayiwa R., Talibawo J., Musoke P., Aturagaba G., Kigozi M. (2025), Activated carbon from banana peels for alizarin removal: understanding the adsorption process through isotherms, kinetics, and predictive modeling. BMC Chem., 19, 301.

Benhadj M., Alouiz I., Amarouch M.Y., Sennoune M. and Mazouzi D. (2023), Wheat Straw-Derived Activated Carbon for Efficient Removal of Methylene blue: Kinetics, Thermodynamics, and Adsorption Mechanism, Key Eng. Mater., 954, 73-93.

Borpujari P., Khan S., Dutta J., Borah D. (2025), Biochar-metal nanocomposites for azo dye removal: Advancements, mechanisms, and future prospects. Discov. Appl. Sci., 7(1), 1023.

Chang S., Wang L., Yao L. (2025), Properties of sunflower straw biochar activated using potassium hydroxide. Molecules, 30, 1332.

Chen G., Yin Y., Zhang X., Qian A., Pan X., Liu F., Li R. (2024), Enhanced adsorption of methyl orange from aqueous phase using chitosan–Palmer amaranth biochar composite microspheres. Molecules, 29, 1836.

de Oliveira M.A., Souza E.S., Correia D.V., Barros B.S., Kulesza J. (2025), Biochar derived from sugarcane bagasse for adsorption of anionic and cationic dyes. Mater. Res., 28(1), e20250179.

Dobele G., Volperts A., Plavniece A., Zhurinsh A., Upskuviene D., Balciunaite A., Niaura G., Colmenares-Rausseo L.C., Tamasauskaite-Tamasiunaite L., Norkus E. (2024), Thermochemical activation of wood with NaOH, KOH and H_3PO_4 for the synthesis of nitrogen-doped nanoporous carbon for oxygen reduction reaction. Molecules, 29(23), 2238.

Dong Y., Liang J., E Z., Song J., Liu C., Ding Z., Wang W., Zhang W. (2024), Preparation of biochar/iron mineral composites and their adsorption of methyl orange. RSC Adv., 14(44), 33977‑33986.

Dukanović N., Apostolović T., Anojčić J., Mutić S., Marjanović Srebro T., Kozma G., Deák C., Maletić S., Beljin J. (2026), Comparative study of biochar from different biomass feedstocks: Toward sustainable resource utilization and environmental applications. Molecules, 31(1), 37.

Feng Z., Fu B., Han S., Yan H., Feng P., Li W., Qin T., Wang T., Zhang X., Jia, J. (2026), Valorization of waste pharmaceutical residues via pyrolysis: Simultaneous production of biochar for Cd^{2+} removal and high-quality bio-oil/syngas. PLOS One, 21(3), e0346024.

Fernandes J.D., Guerra H.O.C., Chaves L.H.G., Laurentino L.G.deS., Cavalcante A.R., Kubo G.T.M. (2022), Thermal treatment of poultry litter: Part II. Evaluation of structural and morphological characteristics. Rev. Bras. Eng. Agríc. Ambient., 26(9), 680-687.

Girish C.R. (2025), Determination of thermodynamic parameters in adsorption studies: a review. Chem. Pap., 79, 5687‑5706.

Guo S., Zou Z., Chen Y., Long X., Liu M., Li X., Tan J., Chen R. (2023), Synergistic effect of hydrogen bonding and π-π interaction for enhanced adsorption of rhodamine B from water using corn straw biochar, Environ. Pollut., 320, 121060.

Gupta A., Dey P. (2025), Hydrothermal and NaOH-treated rice straw fibre: A potential lignocellulosic biosorbent material for removal of textile dyes from contaminated industrial wastewater, Int. J. Biol. Macromol., 305(1), 141109.

Hadi H.J., Ali N.D., Zageer K.F., Ahmed T.A., Al-khateeb R.T., Hassan A.A., Humadi J.I. (2026), Cotton-derived activated carbon/CuO nano-photocatalyst for organic-rich produced water treatment in a digital baffle adsorption–oxidation reactor. Nanotechnol. Environ. Eng., 11, 45.

Hamad H.N., Idrus S., Yusuf B., Jamali N.S., Ahsan A., Suhartini S., Abdul Wahab A.M. (2024), Optimized Bentonite Clay Adsorbents for Methylene Blue Removal, Processes, 12(4), 738.

Hassan A.A., Nawaf A.T., Al-khateeb R.T., Humadi J.I. (2026), Design and synthesis of Ag_2O/bentonite composite for enhanced adsorption and photodegradation of organic compounds. Water Air Soil Pollut., 237, 905.

Humadi J.I., Nawaf A.T., Khamees L.A., Abd-Alhussain Y.A., Muhsin H.F., Ahmed M.A., Ahmed M.M. (2023), Development of new effective activated carbon supported alkaline adsorbent used for removal phenolic compounds. Commun. Sci. Technol., 8(2), 164‑170.

Issa Y.S., Mahmood Q.A., Humadi J.I., Hassan G., Haldhar R. (2025), Design of new wet heterogeneous photo oxidation process for refinery waste water treatment in photo baffled reactor. Water Air Soil Pollut., 236(1), 70.

Jamil U., Zeeshan M., Khan S. R., Saeed S. (2023), Synthesis and two-step KOH based activation of porous biochar of wheat straw and waste tire for adsorptive exclusion of chromium (VI) from aqueous solution; thermodynamic and regeneration study. J. Water Process Eng., 53, 103892.

Li G., Zhang F., Ma Y., Zhang X., Liu Q., Ye R., Ma Y., Liu X. (2025), Enhanced stabilization of lead in soil using novel biochar composites under simulated accelerated aging conditions. Sustainability, 17(6), 2563.

Li Z., Chen X., Qiu L., Xu H., Fan L., Meng S., Jiang Z., Song C. (2025), N-Doping/KOH synergy in waste moss biochar for geosmin removal in aquaculture water: Elucidating surface functionalization and activation mechanisms. Biology, 14, 1045.

Limmun W., Limmun W., Maneesri W., Pewpa O., Chungcharoen T., Ishikawa N., Borkowski J. J., Ito A. (2025), Sustainable tropical fruit peel waste biochars for enhanced cadmium and lead adsorption: mechanistic insights and optimization using response surface methodology and backpropagation neural networks. Biomass Convers. Biorefin., 15(16), 23321-23343.

Liu H., Zhu J., Li Q., Li L., Huang Y., Wang Y., Fan G., Zhang L. (2023), Adsorption Performance of Methylene Blue by KOH/$FeCl_3$ Modified Biochar/Alginate Composite Beads Derived from Agricultural Waste, Molecules, 28, 2507.

Liu P., Gerometta M., Pizzi A., Fierro V. (2024), KOH activation mechanism in the preparation of brewer’s spent grain-based activated carbons. Catalysts, 14, 814.

Liu W., Huang J., Weatherley A.J., Zhai W., Liu F., Ma Z., Jiao Y., Zhang C., Han B. (2022), Identifying adsorption sites for Cd(II) and organic dyes on modified straw materials, J. Environ. Manag., 301, 113862.

Loebsack G., Yeung K.K.C., Berruti F., Klinghoffer N.B. (2025), Impact of biochar physical properties on adsorption mechanisms for removal of aromatic aqueous contaminants in water. Biomass and Bioenergy, 194, 107617.

Lotfy V.F., Basta A.H. (2026), Sustainable heteroatom doped biochar for methylene blue adsorption with structure function insights. Sci. Rep., 16, 13135.

Lucas M.S., Teixeira A.R., Jorge N., Peres J.A. (2025), Industrial wastewater treatment by coagulation‑flocculation and advanced oxidation processes: A review. Water, 17(13), Article 1934.

Majd M.M., Kordzadeh-Kermani V., Ghalandari V., Askari A., Sillanpaa M. (2022), Asorption isotherm models: A comprehensive and systematic review (2010-2020). Sci. Total. Environ., 812, 151334.

Martínez R.J., Vela-Carrillo A.Z., Godínez L.A., Pérez-Bueno J.J., Robles I. (2023), Competitive adsorption of anionic and

cationic molecules on three activated carbons derived from agroindustrial waste, Biomass Bioenergy, 168, 106660.

Mim S., Hashem M.A., Payel S. (2023), Coagulation-adsorption-oxidation for removing dyes from tannery wastewater, Environ. Monit. Assess., 195(6), 695.

Minaei S., Benis K.Z., McPhedran K.N., Soltan J. (2024), Adsorption of sulfamethoxazole and lincomycin from single and binary aqueous systems using acid-modified biochar from activated sludge biomass. J. Environ. Manag., 358, 120742.

Moharm A.E., El Naeem G.A., Soliman H.M.A., Abd-Elhamid A.I., El-Bardan A.A., Kassem T.S., Nayl A.A., Bräse S. (2022), Fabrication and Characterization of Effective Biochar Biosorbent Derived from Agricultural Waste to Remove Cationic Dyes from Wastewater, Polymers, 14(13), 2587.

Mohammed A.E., Abdullah G.H., Yousif S.H., Humadi J.I. (2026), Catalytic degradation of phenol from refinery wastewater using hybrid oxidation-adsorption in multi fixed-bed reactor: Experimental and kinetic study. J. Water Process Eng., 83, 109558.

Nandi R., Jha M.K., Guchhait S.K., Sutradhar D., Yadav S. (2023), Impact of KOH activation on rice husk derived porous activated carbon for carbon capture at flue-gas-alike temperatures with high CO_2/N_2 selectivity. ACS Omega, 8, 4802–4812.

Nascimento F.H., Infante C.M.C., Pereira E.A.O., Leite S.T., Masini J.C. (2023), Empirical Adsorption Kinetics: Comparing Linear and Nonlinear Regression Analysis Emphasizing the Need for High Throughput Analysis, J. Environ. Sci. Health. Part B, 58 (7), 539‑553.

Nawaf A.T., Hassan A.A., Mohammed H.K., Humadi J.I. (2026a), Improving water quality by whole wates water treatment: Solar Fenton oxidation process in a new design digital baffle Fenton-solar batch reactor. Coke Chem., 69(3), 173–181.

Nawaf A.T., Abdullah G.H., Humadi J.I., Saeed L.I., Mohammed M.H., Habila M.A., Haldhar R. (2026b), Novel photo catalytic baffled reactor for eco-friendly and deep diesel desulfurization process using magnetic heterogeneous catalyst. Water Air Soil Pollut., 237, 88.

Nguyen T.P.T., Pham T.L.N., Huynh K.-P.-H., Dang B.-T. (2025), Comparison of porous and non-porous biochar for trimethoprim removal: Quantifying uncertainty in sorption and thermodynamic parameters over different pH and temperature. Case Stud. Chem. Environ. Eng., 12, 101264.

Onyango C., Nyairo W., Tchieta G.P., Shikuku V.O. (2025), Watermelon rind based adsorbents for the removal of water pollutants: A critical review. Front. Environ. Chem., 6, 1568695.

Rangasamy G., Rathi B.S., Kumar K.S., Murugeshwari S., Lalitha S.M., Kumar P.S. (2026), Hydrothermal carbonization derived hydrochar from industrial waste as an efficient adsorbent for toxic dye removal and process optimization. Sci. Rep., 16, 3280.

Reçber Z. (2022), Adsorption of methylene blue onto spent alchemilla vulgaris leaves: characterization, isotherms, kinetic and thermodynamic studies, Int. J. Environ. Sci. Technol., 19(6), 4803-4814.

Saranya M., Gomathi T., Pavithra S., Mubashirunnisa A., Sudha P.N. (2022), Batch kinetic studies of adsorption of Cu(II) ions from aqueous solutions onto alginate nanoparticles/PEG binary blend, Indian J. Mar. Sci., 51(05), 484-489.

Senapati S., Giri J., Mallick L., Singha D., Bastia T. K., Rath P., Rana M. K., Panda A. K. (2025), Rapid adsorption of industrial cationic dye pollutant using base-activated rice straw biochar: Performance, isotherm, kinetic and thermodynamic evaluation. Discov. Sustain., 6(1), 46.

Shah V.V., Patel N.M. (2026), Circular economy pathway: Valorization of cotton stalk into biochar for textile wastewater treatment. Environ. Nat. Resour. J., 24(2), 250–267.

Sharshoh M.A., Shihab M.A., Hadic H.J., Humadi J.I., Nawaf A.T., Hassan A.A., Jafar S.A. (2026), Hybrid adsorption/UV-driven photocatalytic oxidation for fast removal of Direct Red dye from industrial wastewater: Experimental work and modeling. Prot. Met. Phys. Chem. Surf., 62(1), 1–14.

Silva J.A. (2025), Advanced oxidation process in the sustainable treatment of refractory wastewater: A systematic literature review. Sustainability, 17(14), 3439.

Song L., Li Y., Lei T., Yang Y., Shen Y., Yang M., Wang Y., Zheng H. (2025), Research on the water absorption diffusion model and kinetics of pretreated straw, Sci. Rep., 15, 9927.

Soudagar S., Akash S., Venkat M.S., Poiba V.R., Vangalapati M. (2022), Adsorption of methylene blue dye on nano graphene oxide-thermodynamics and kinetic studies. Mater, Today: Proc., 59(1), 667-672.

Strebel A., Behringer M., Hilbig H., Machner A., Helmreich B. (2024), Anionic azo dyes and their removal from textile wastewater through adsorption by various adsorbents: A critical review. Front. Environ. Eng., 3, 1347981.

Tang Y., Li Y., Zhan L., Wu D., Zhang S., Pang R., Xie B. (2022), Removal of emerging contaminants (bisphenol A and antibiotics) from kitchen wastewater by alkali-modified biochar, Sci. Total. Environ., 805, 150158.

Tomin O., Vahala R., Yazdani M.R. (2024), Synthesis and efficiency comparison of reed straw-based biochar as a mesoporous adsorbent for ionic dyes removal. Heliyon, 10, e24722.

Trazzi P.A., Vashishtha M., Najser J., Schmalenberger A., Kannuchamy V.K., Leahy J.J., Kwapinski W. (2024), Adsorption of ammonium, nitrate, and phosphate on hydrochars and biochars. Sci. Adv., 14(6), 2280.

Ud Din S., Ngueagn P.T., Al-Ahmary K.M., AlMohamadi H., Al-Mhyawi S.R., Elamin N.Y., Alshdoukhi I.F., Alrashood J.S., Ofudje E.A. (2025), Adsorption of Bisphenol-A by banana biochar: kinetic, isotherms and thermodynamics. Sci. Rep., 15, 31659.

Vasilievici G., Sanda M., Băjan M., Dușescu-Vasile C., Onutu I., Brănoiu G., Bomboș D., Baioun A., Borcea A.F., Stănică A.I. (2025), Synthesis and characterization of biochar obtained by partial delignification of waste biomass. Molecules, 30, 4505.

Vásquez Llanos, S.A., Sausa Burga L.L., Guevara Fernández D.N., Sánchez Purihuaman M.N., Huangal Scheineder S., Carreño-Farfan C.R., Vivas-Cuellar M.C., Rivadeneira Sipion K., Medina Collana J.T., Barturén Quispe A.P. (2025), Rice husk biochar as a sustainable adsorbent for tetracycline removal from aqueous solution by using Taguchi design approach. J. Ecol. Eng., 26(9), 382‑399.

Wang H., Du Y., Song Y., Zhang H. (2025), Preparation, characterisation and adsorption performance of KOH-modified palm fibre, platanus bark and sesame stem biochar, Int. J. Environ. Sci. Technol., 22, 2613‑2624.

Wang J., Guo X. (2022), Rethinking of the intraparticle diffusion adsorption kinetics model: Interpretation, solving methods and applications, Chemosphere, 309(2), 136732.

Wang S., Chen Y., Ge S., (2023), Adsorption characterization of tetracycline antibiotics on alkali-functionalized rice husk biochar and its evaluation on phytotoxicity to seed germination, Environ. Sci. Pollut. Res. Int., 30(58), 122420-122436.

Wang Y., Huo T., Wang Y., Bai J., Huang P., Li C., Deng S., Mei H., Qian J., Zhang X., Ding C., Zhang Q., Wang W. (2024), Constructing mesoporous biochar derived from waste carton: Improving multi-site adsorption of dye wastewater and investigating mechanism. Environ. Res., 242, 117775.

Wei F., Jin S., Yao C., Wang T., Zhu S., Ma Y., Qiao H., Shan L., Wang R., Lian X., Tong X., Li Y., Zhao Q., Song W. (2023), Revealing the Combined Effect of Active Sites and Intra-Particle Diffusion on Adsorption Mechanism of Methylene Blue on Activated Red-Pulp Pomelo Peel Biochar, Molecules, 28(11), 4426.

Xu J., Zhang Y., Li B., Fan S., Xu H., Guan D. (2022), Improved adsorption properties of tetracycline on KOH/$KMnO_4$ modified biochar derived from wheat straw, Chemosphere, 296, 133981.

Yahya M.A., Al-Qodah Z., Ngah C.W.Z., Hashim M.A. (2015), Preparation and characterization of activated carbon from desiccated coconut residue by potassium hydroxide. Asian J. Chem., 27(6), 2331–2336.

Yahya M.A., Ngah C.W.Z., Hashim M.A., Al-Qodah Z. (2016), Preparation of activated carbon from desiccated coconut residue by chemical activation with NaOH. J. Mater. Sci. Res., 5(1), 24‑31.

Yu H., Zhang Y., Wang L., Tuo Y., Yan S., Ma J., Zhang X., Shen Y., Guo H., Han L. (2024), Experimental and DFT insights into the adsorption mechanism of methylene blue by alkali-modified corn straw biochar. Electronic supplementary information (ESI) available, RSC Adv., 14(3), 1854-1865.

Yu W., Xie Z., Zhang N., Tang L., Xia J., Ye J., Liu X., Wang D., Yang G. (2025), Sustainable optimization of high specific surface area Spartina alterniflora biochar for Rhodamine B removal and mechanism. Sci. Rep., 15, 21745.

Zhai Q. (2023), Adsorption of Rhodamine B dye on potassium permanganate modified peanut shell: adsorption kinetics, thermodynamics and isotherm studies, Desalin. Water Treat., 303, 212-223.

Zhang X., He Z., Jia W., Meng F., Zhang W., Lu C., Hao X., Gai G., Huang Z., Xu M., Wang K., Yun S. (2024), Mechanism of potassium release from feldspar by mechanical activation in presence of additives at ordinary temperatures. Mater., 17(14), 1701044.

Zhang X., Zhang X., Xu W. (2025), Adsorption performance and mechanism of waste Myriophyllum aquaticum biochar for malachite green in wastewater: Batch and column studies. Sustainability, 17(12), 2868.

Zhao F., Shan R., Li S., Yuan H., Chen Y. (2023), Characterization and Co-Adsorption Mechanism of Magnetic Clay-Biochar Composite for De-Risking Cd(II) and Methyl Orange Contaminated Water, Int. J. Mol. Sci., 24(6), 5755.